THE GROWTH OF SINGLE CRYSTAL OF ZINC SELENIDE

TOSHIYUKI KURIKI, MASAKAZU OHISHI and KENZO OHMORI

Department of Applied Physics, Okayama College of Science, Okayama, Japan.

(Received September 30, 1974)

ABSTRUCT

ZnSe single crystal is made by the Bridgeman method under high inert gas pressure and its crystallographic characteristics are described. The lattice parameter of grown crystal is 5.667 ± 0.003 Å and the twin structures along the $\langle 111 \rangle$ directions are observed. There are two kinds of {111} planes in zinc blend type compounds, one is designated as {111} surfaces or A surfaces and the other as $\{\bar{1}\bar{1}\bar{1}\}$ surfaces or B surfaces. Their differences are determined by means of the anomalous dispersion of X-ray and are discussed in relation to etch patterns.

§. 1. INTRODUCTION

As II-VI, III-V compounds (ZnS, ZnSe, CdS and GaP etc.) decompose into their voltatile components far below their melting points, these single crystals have been grown mostly by chemical tranport and vapour phase methods so far. The procedure of growing by these methods is very troublesome, taking a long time, and yet the grown crystal is small. However, if the vapour pressure is suppressed by high pressure, it is possible to grow the single crystal from the melt. A. G. Fisher has given a full detail of the crystal growth of the decomposable materials from the melt under pressure by variety methods[1]. The high pressure, high temperature electric furnace, developed by Gakei Electric works Co. Ltd., can be used as both Bridgeman and Tamman methods. The crystallization by means of the electric furnace of this type are reposted by many investigators, such as ZnS by S. Shionoya[2], EuS by T. Nakayama *et al*[3]., ZnSe by S. Ibuki *et al*[4]. and S. Fukai *et al*[5]..

The authors have succeeded in crystallizing ZnSe single crystal by Bridgeman method with good reproducibility. Advantages of Bridgeman method from the melt under high inert gas pressure are as follows :

(1) The growth perioid is shorter than the other methods (chemcal transport, growth from vapour phase).

(2) The large single crystal can be grown.

(3) Incorporation of impurities are easy.

(4) Good reproducibility.

(5) The homogenious crystal can be obtained.

(6) The crystallization of solid solution is possible.

Before the measurement of optical and electrical properties, their surfaces are investigated. ZnSe has a zinc blend structure which is the same as that of diamond except for the alterna-

tion of the two different elements on successive lattice sites. Their space group is denoted as $F\bar{4}3m(Td_2)$. The surfaces of compounds with zinc blend structure exhibit their own different characteristics, *i. e.*, the crystal growth, the etch pits formation and the gas adsorption as a result of the crystallographic polarity along the $\langle 111 \rangle$ directions. The surfaces {111} terminating with group II atoms (Zn) are designated as the {111} surfaces or the A-surfaces, and those terminating with group VI atoms (Se) are designated as the $\{\bar{1}\bar{1}\bar{1}\}$ surfaces or the B surfaces. The method of determination of polarity is reviewed by T. Ogawa[6] and the practical examples on III-V and II-VI compounds except for ZnSe can be seen in the reports by H. C. Gatos and E. P. Warekois et al.[7,8] The present paper describes the vertical Bridgeman growth method for ZnSe single crystals from the melt under pressure. In order to investigate the crystallographic characteristics of grown crystals, X-ray diffraction patterns, etching behaviours of {110}, {111} surfaces and crystallographic polarity of the {111} surfaces are studied. Furthermore, discussions are made on light figures, one of the conventional methods to determine the orientation of the crystal.

§. 2. CRYSTAL GROWING METHOD

The photograph of the electric furnace made by Gakei Electric Works Co. Ltd. is shown in Fig. 1. This furnace is filled with Ar gas and kept about 120 kg/cm^2 during crystal growth.

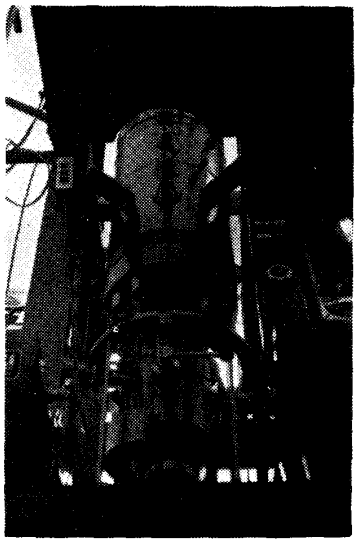

Fig. 1. Photograph of the high presure, high temperature electric furnace.

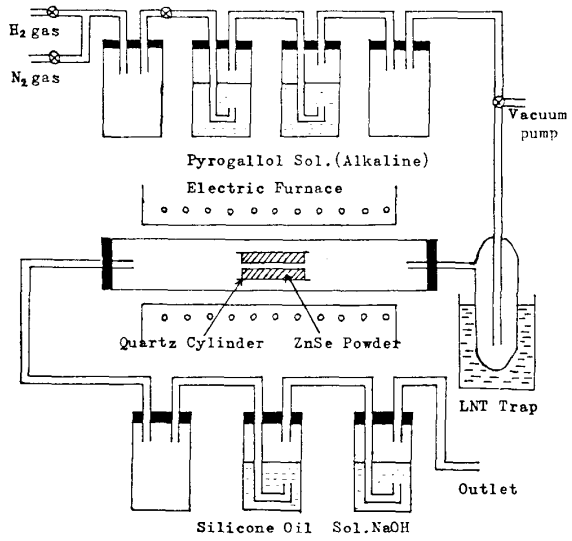

Fig. 2. Apparatus used for the refining of ZnSe powder.

The starting material (luminescent grade ; 99.999 % purity ; Sakai Chem. Co. Ltd.) is refined in the flowing H_2 gas at 1000°C for about 1 hour. Fig. 2. illustrates the apparatus used for this refining. The weight of the refined powder decreased to 80 % of the initial weight and the color of the powder turned from brown to bright yellow. By this refining the excess selenium, ZnO and H_2O are excluded quite well, and the powder is completely crystallized into zinc blend structure.

The crucible (made of graphite ; shown in Fig. 3) which influences on the purity of the crystal must be carefully refined. The adopted procedures are as follows :

(1) Baked in the atomosphere of Ar gas at 1000°C for 1 hour.

(2) Immersed in the aqua-regia for 24 hours.

(3) Etched in the solution (100cc HNO_3+10cc HF +90cc H_2O) at 100°C for 12 hours.

(4) Rinsed in the distilled water at 70-80°C for 8 hours (repeated 4 times)

(5) Dried in the oven at 200°C for 24 hours.

(6) Baked in the vacuum at 1000°C for 1 hour.

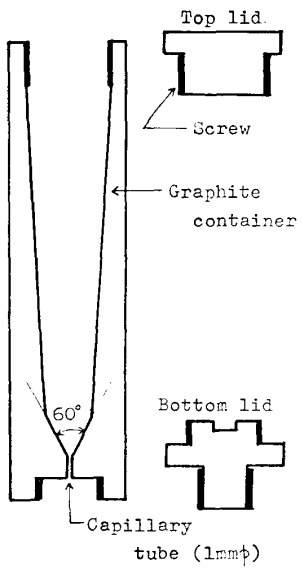

Fig. 3. Form of the graphite crucible.

The heating of high pressure furnace is carried out by P-I-D method with saturable core reactor. The crucible is maintained for 15-30 min. above the melting point (1520°C[9]) in order to be completely melted, then the crucible is pulled down from outside of the furnace by a magnetic coupling mechanism at an appropriate rate from about 1550°C to 800°C and the power is cut off. The temperature of the crucible is measured by thermocouple (W-5% Re/W-26% Re) which is attached to 18 mm under the end part of it. The temperature distribution in the furnace is shown in Fig. 4, and the temperature gradient caluculated from Fig. 4. is shown in Fig. 5. These curves are

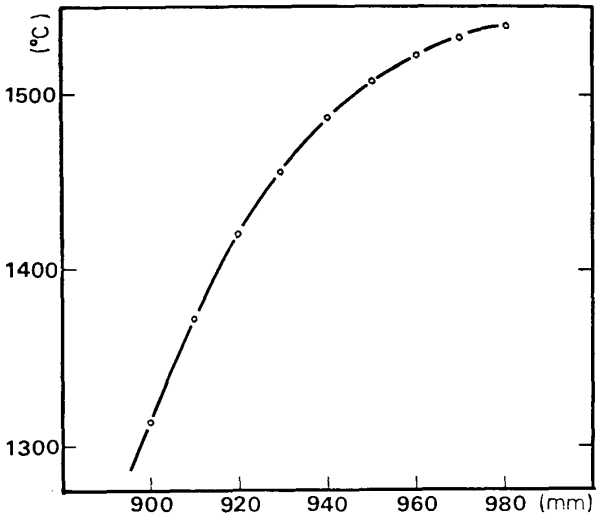

Fig. 4. Temperature distribution in the furnace measured by W-5% Re/W-26% Re thermocouple.

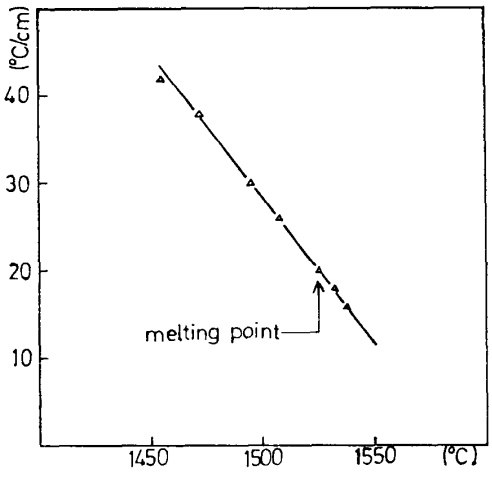

Fig. 5. Temperature gradient as a function of temperature. (calculated from Fig. 4)

uniquely determined by the heater shape and its surroundings, therefore the controllable factors which influence the crystal growth are the shape of crucible, gas pressure and the pulling down rate. In these factors the crucible is so influential on the crystallization that their inner wall is formed into the particular shape shown in Fig. 3. The capillary tube (1 mm ϕ) at the inner bottom promote the crystal growth of preferable orientation. By

Fig. 5., the temperature gradient near the melting point is about 20°C/cm, which is a little smaller than the reported value[4]. Crucible temperature measured during crystal growth is shown in Fig. 6. Pulling down speed 18-36 mm/hour gives the single crystal without polycrystalline with good reproducibility. The evaluated temperature change per minute is represented in Fig. 7., which is all below 1°C /min. near the melting point. If the crucible

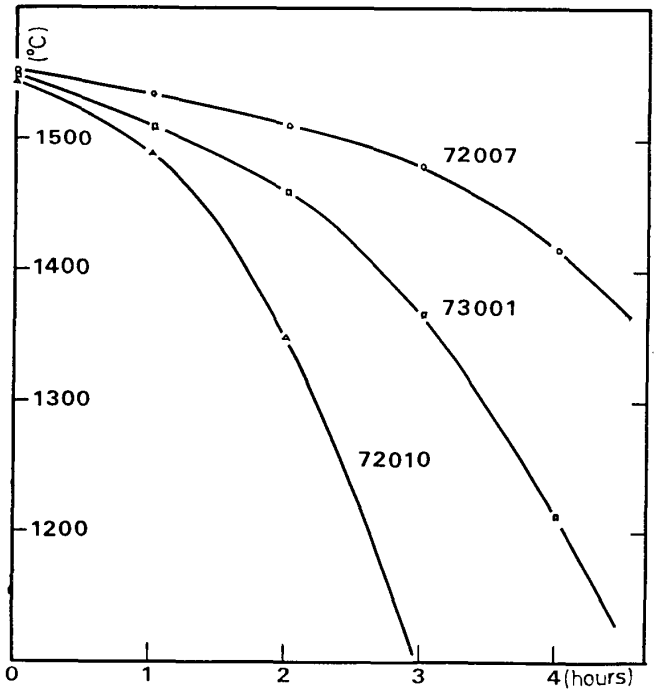

Fig. 6. Crucible temperature measured during crystal growth.

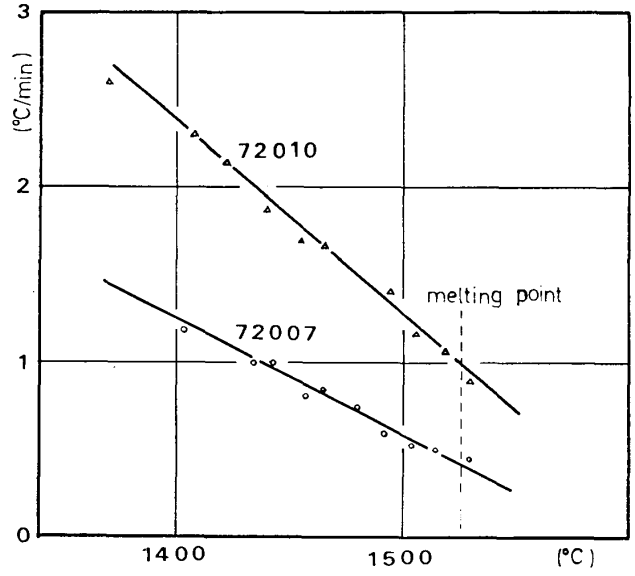

Fig. 7. Temperature change per minute of the crucible.

is pulled down at a speed below 18 mm/hour, the large single crystal is not grown since Bridgeman method becomes similar to Tamman method and furthermore the deviation from the stoichiometry is caused in the long run. On the other hand, if the crucible is pulled down fastly (more than 35 mm/hour), the polycrystal is also grown since the equilibrium between the solid and liquid phases is not established. It is reported that the yield (grown crystal weight/charged weight) is less than 20 % and that grown crystal is polycrystalline under the pressure of 10 kg/cm^2 in the case of ZnSe[4]. The yield in our laboratory was about 90 % in the region from 90 to 120 kg/cm^2 and pressure had no remerkable effect on crystal growth. The direction of crystal growth was almost the ⟨100⟩, but the ⟨110⟩ and the ⟨111⟩ were observed sometimes. Generally speaking, the growth to ⟨110⟩ and ⟨111⟩ directions have the tendency to become polycrystalline. The obtained crystal is shown in Fig. 8., its size is about 17 mm in diameter and 65 mm in length. The as-grown crystal etched weakly in NaOH solutin has the regular stripe patterns and the lapped crystal is orange-yellow in color except the end part and transparent. These stripes become disorder in polycrystalline ingot and are not observed in the worst condition. In such a case the crystal color is nearly blackish red. As-grown crystal has high resistivity (higher than 10^{10} Ω-cm) and slightiy orange luminescence

is observed only at liquid nitrogen temperature by stimulating Hg 3650 Å line. The crystals anealed in the molten zinc (solvent extraction method[10]) show luminescence even at room temperature and their resistivity become few Ω-cm. The crystals used for the following experiment are all as-grown crystals.

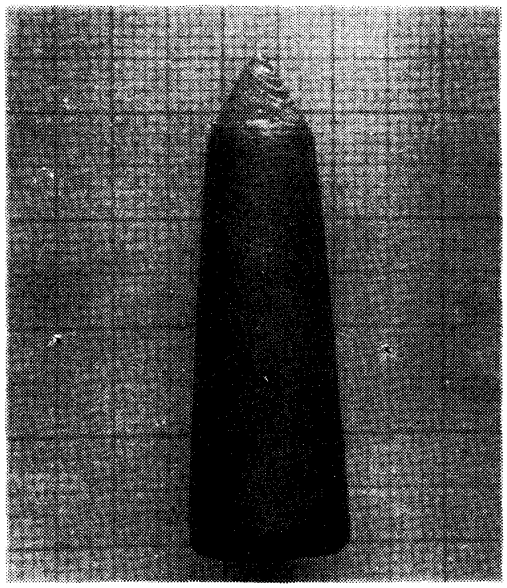

Fig. 8. Form of as-grown crystal of ZnSe (etched with NaOH solution).

§. 3. X-RAY ANALYSIS OF GROWN CRYSTAL

In order to investigate the grown crystal, X-ray diffraction patterns are examined about the raw material, refined powder and single crystal of ZnSe (Fig. 9). The raw material has the broad diffracted lines (Fig. 9-(a)), which means crystallization is not satisfactory. According to the qualitive fluorescent X-ray analysis, the raw material contains many impurities, such as K, Ca, Cl, Fe and S etc. In these impurities, S which would be incorporated in the process of synthesis of the ZnSe powder is predominant in quantity. The refined material show sharp diffraction lines of zinc blend type, and it is noted that they have a few hexagonal components, ZnO and other unknown materials. As far as X-ray analysis are concerned, the diffraction patterns of single crystal show no hexagonal components and oxides except for the end part of the crystal (Fig. 9-(c), (d)), which would be excluded during crystal growth. The evaluated lattice constant of ZnSe single crystal is 5.668 ± 0.003 Å, which is consistent with other reported results[11-13]. The impurities contained in the single crystal are comparable to the refined powder by means of fluorescent X-ray analysis, so that the great care must be taken to the refining process of ZnSe powder and the cleaning of the crucible. It is very effective method for the exclusion of sulfur from the raw material to bake in the flowing H_2 gas. The back Laue photographs of the cleaved {110} and the lapped {111} planes are shown in Fig. 10. Both patterns do not show the patterns of single crystal. The pattern of the {110} plane is 4-fold symmetry but not 2-fold symmetry and that of the {111} plane is 6-fold but not 3-fold. These facts suggest that the crystal contains twins and their twin axis are the $\langle 111 \rangle$ directions. So the {110} planes are composed of the (110) and $(\bar{1}\bar{1}0)$

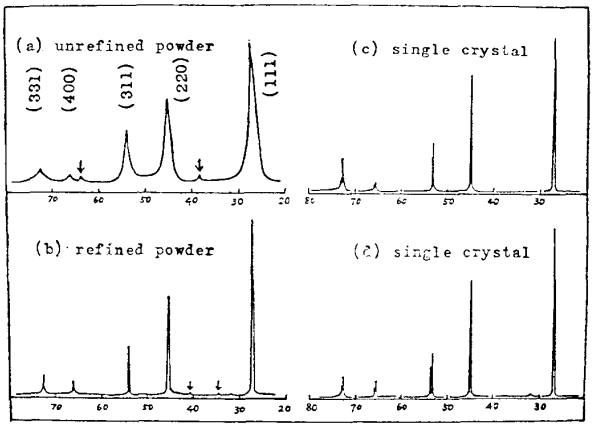

Fig. 9. X-ray diffraction patterns (Cu K_α radiation)
(a) raw material (b) refined in the H_2 gas
(c) bottom part of single crystal
(d) upper part of single crystal.

planes. But if the {111} planes are cut perpendicular to the cleaved {110} planes, the plane without twin can be obtained. This is to be discussed later in detail.

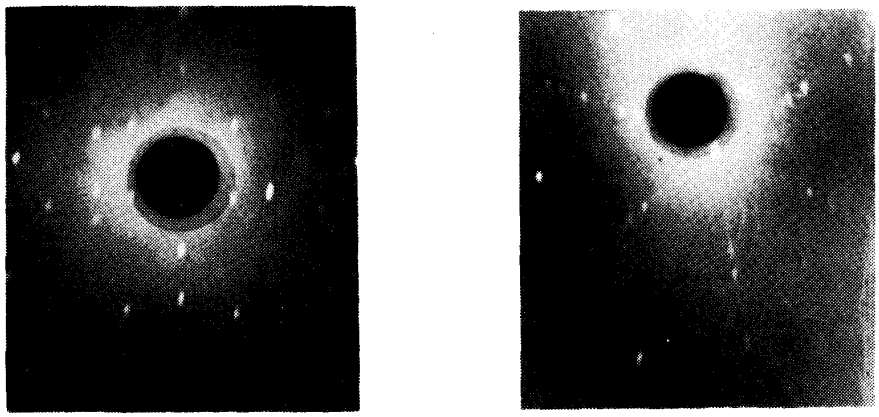

(a) (b)

Fig. 10. Back Laue photographs of (a) {110} and (b) {111}.

§. 4. ETCHING BEHAVIOURS OF ZnSe SINGLE CRYSTAL

(1) *Etch patterns and light figures of the* {110} *surfaces.*

The etchant used in this experiment is the solution of 30 g NaOH+70 g H_2O. The other acid reagents, such as 1 (part by volume) conc HCl+1 conc HNO_3, HF *etc*, are examined, but NaOH reagent is the most suitable for the pits formation of ZnSe single crystal. The cleaved surface {110} of ZnSe after etching at 110-120°C shows many small isosceles triangles as shown in Fig. 11. (a), (b), (c). Their base directions change at the parallel lines composed of high pits density on this plane, which are the crossing of the {110} and {111} planes. Refering to Laue photographs, the side direction of the triangles in etch pattern is 〈111〉

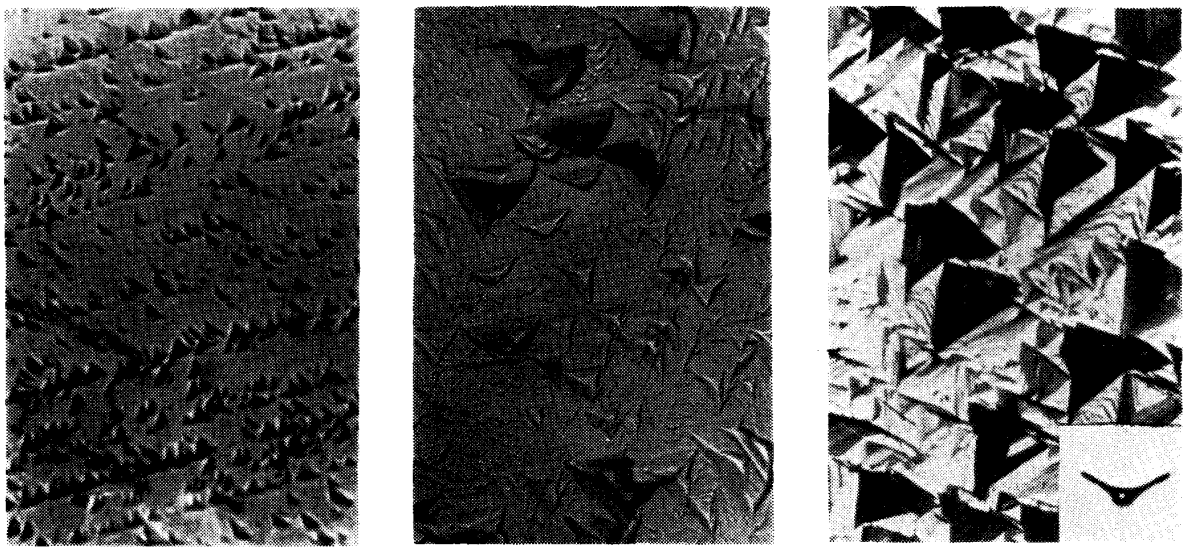

(a) (b) (c)

Fig. 11. Etch figures of {110} (approx. × 400) ; etching time
(a) 2 min. (b) 5 min. (c) 10 min.

and the base direction is ⟨110⟩. The two types of triangular pits are not in the relation of the mirror reflection but the rotary reflection, that is, the etch pits are rotated 180° through the ⟨111⟩ twin axis.

As the observed angles of the triangular pits agree satisfactorily with caluculated ones, if the pits orientations are determined with the X-ray photographs, the crystal orientation can be determined easily by the pits observation. When a cleaved faces are etched progressively, pits grow and combine at the twin boundary and their outlines become equilateral triangular pits. These pits growth can be explaned by the difference of the chemical activitiy of the {111} and $\{\bar{1}\bar{1}\bar{1}\}$ surfaces. To show the coincidence, their etch patterns of the pair of cleaved faces are shown in Fig. 12 (a), (b). Not only the twin boundaries but also the large pits might be caused by the inclusion matches closely on opposite side of cleaved surface. The pits density calculated from Fig. 11 (a) is about $1\times10^7/cm^2$ and from Fig. 11 (c) $2\times10^3/cm^2$. The twin density evaluated by the number of the twin boundaries per cm is between 600/cm and 1500/cm along the ⟨111⟩ directions. One of the determination methods for crystal orientation is to examine the light figure[14]. The light figures are obtained from the {110} surfaces etched heavily. The pattern shows two strong lines and a weak one. The weak line direction, that is, the bisector of the strong lines corresponds to the ⟨111⟩ directions (Fig. 11 (c)). For the slightly etched crystal, the light figure is not observed since the reflected beam is weak.

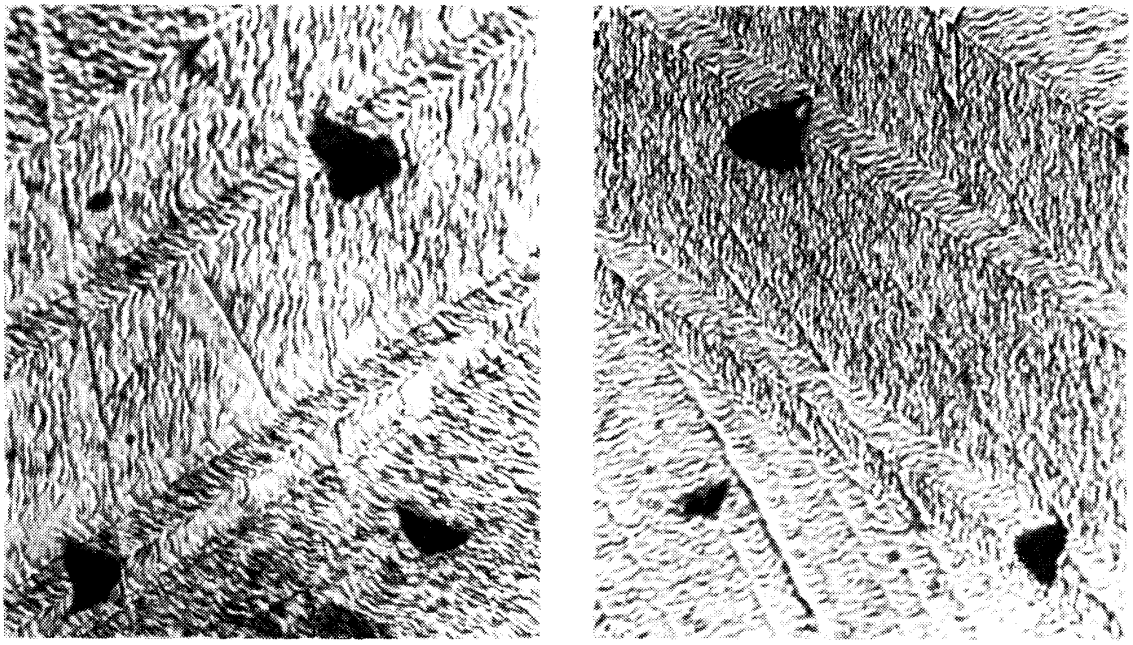

(a) (b)

Fig. 12. Etch figures of pair of cleaved {110} surfaces. (approx. × 400)

(2) *Etch patterns and light figures of the* {111} *surfaces.*

The {111} surfaces of ZnSe after etched for 5 min. develop the triangular pits as shown in Fig. 13. There are two kinds of pits, sharp pits and diffuse ones. II-VI compounds

with zinc blend structure have the geometrical polarity along the ⟨111⟩ directions, i.e., the {111} and {$1\bar{1}\bar{1}$} surfaces are nonequivalent to each other and exhibit the physical and chemical properties of their own.

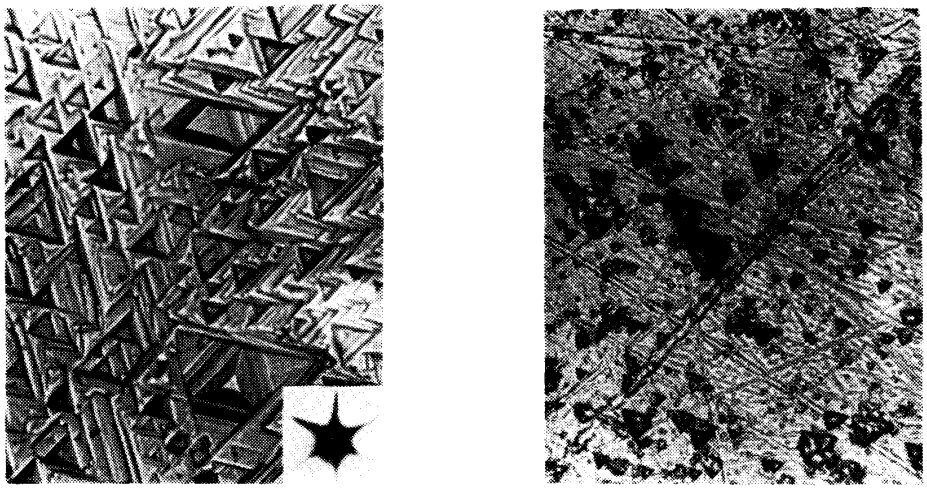

(a) (b)

Fig. 13. Etch figures of (a) {111} and (b) {$\bar{1}\bar{1}\bar{1}$} surfaces. (approx. × 400)

In zinc blend structure the atomic stacking sequences can be represented as -A-B-C-A-B-C- *etc.* (Fig. 14[15]). If the crystal contains the twins, this stacking is changed to -A-B-C-B-A-C------B-A-B-C-A-B-C- *etc.*

The symbol ↓ shows the composition surfaces. At the twin planes, the crystal rotates 180° through the ⟨111⟩ twin axis and the atomic arrangements of -Zn-Se-Zn-Se-Zn-Se- *etc.* along the ⟨111⟩ directions are conserved. So the distance between the first neighbours is equal.

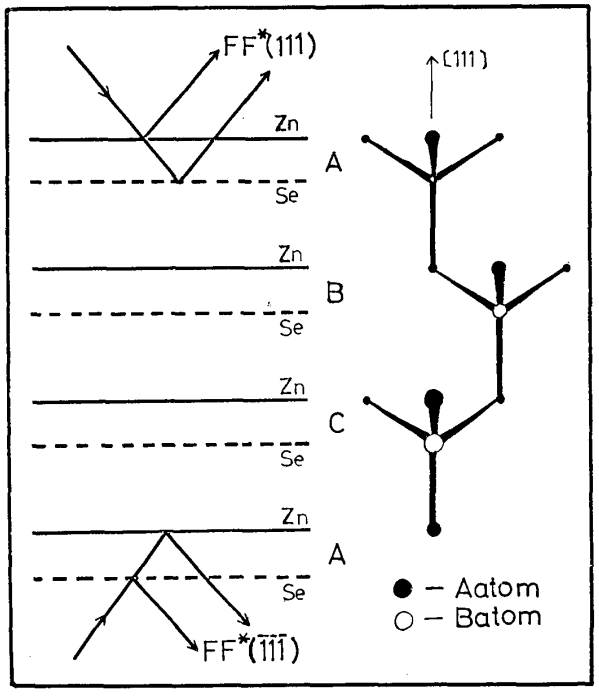

Fig. 14. Atomic stacking of zinc blend structue.

If the crystal is cut parallel to this {111} surfaces, the crystal of which surfaces have not twin is obtained.

The delta, nabra and overlaped pits appear clearly in Fig. 13 (a). These features can be explaned by considering inaccuracy of cutting, thickness of the twinlamellae and the high etching rate. On the other hand, the etch pits of the Fig. 13 (b) (the opposite side shown in Fig. 13 (a)) have small delta pits only and the damages formed in the process of polishing are present yet. Etching rate of this surfaces is small, comparing with those of Fig. 13(a) for the same etchant. As the etching time

increases, the former surfaces (Fig. 13 (a)) become gradually mirror-like and then the flat bottomed pits disapear. Finally all remained pits become the shape of pyramid-like and their density decreases to about $5\times10^2/cm^2$. Whereas the latter surfaces (Fig. 13 (b)) remain rough and nonreflective, and pits or strucrure are recognized no longer (Fig. 15 (a), (b)). The surfaces etched with 1 (part by volume) conc. HCl+1 conc. HNO_3 show nearly the same characteristic patterns as those etched with NaOH etchant, that is, one is shallow rouneded pits and the other a nondescript structure (Fig. 16). The fact that the pits are mainly produced only at one side of {111} is consistent with one that the dislocation pits are recognized in Zn plane in the cases of ZnS and ZnTe[7]. In order to determine the crystallographic polarity of ZnSe, it is necessary to examine by means of anomalous dispersion of X-rays.

The light figure from the surfaces with sharp triangular pits is shown in Fig. 13 (a). This 6-fold symmetric pattern is expected from the etch pits shapes and consistent with the

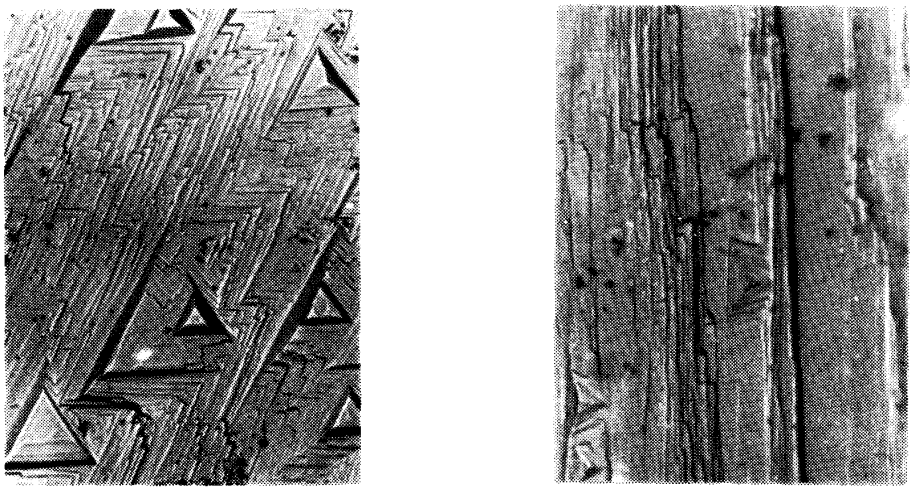

(a) (b)

Fig. 15. Etch figures of the $\{111\}_{Zn}$ surfaces. (a) 10 min. etched (b) 20 min. etched. (approx. ×400)

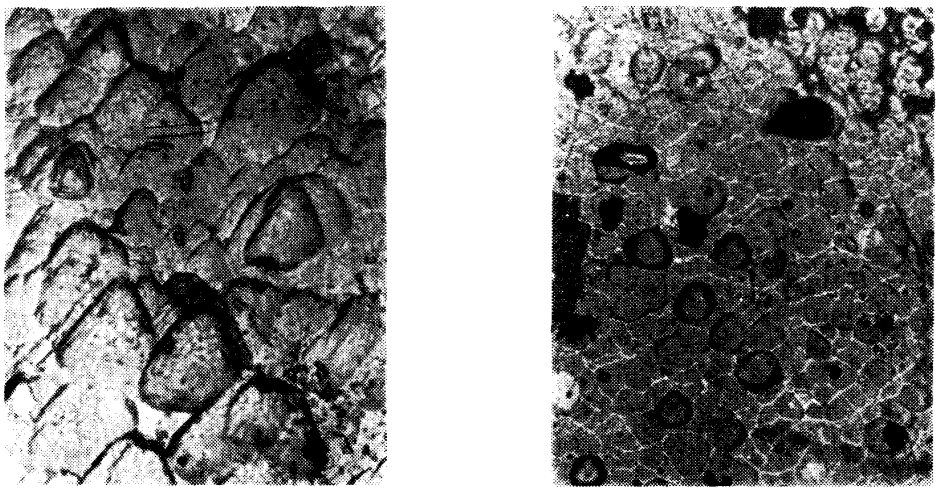

(a) (b)

Eig. 16. Etch figures of the {111} surfaces produced with 1 (part by volume) conc. HCl+1 conc. HNO_3. (a) $\{111\}_{Zn}$ surfaces (b) $\{\bar{1}\bar{1}\bar{1}\}_{Se}$ surfaces. (approx. × 400)

results of back Laue photographs. The light figure of the other {111} surfaces can not observed because of the etch pits diffuseness and shallowness.

§. 5. DETERMINATION OF POLARITY

Recenty it has been investigated that the identification of crystallographic polarity in II-VI compounds by employing X-ray diffraction and also correlated the etching characteristics of their A and B surfaces with X-ray identification by H. C. Gatos *et al*[8].. But they are not refered to ZnSe at all. In order to assign the polarity of ZnSe surfaces, the conventional fluorescent X-ray spectrometer (Rigaku ; Geiger Flex SX) was used. As the analysing crystal the {111} planes of ZnSe were used and KBr+RbCl, Ge single crystal and Cu metal were employed as characteristic X-ray sources. The schematic arrangements for the measurement are shown in Fig. 17.

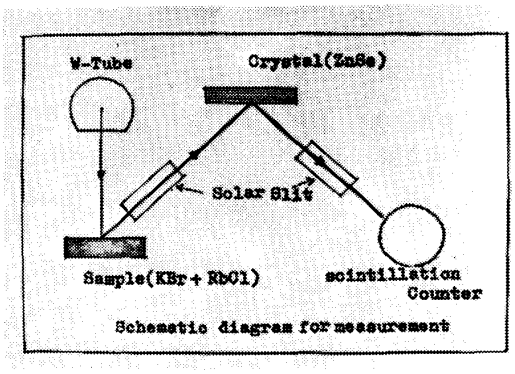

Fig. 17. Experimental set up for polarity measuremnt.

The proccedure of the calculation of the diffracted intensities are as follows,

$$F\,(hkl) = \sum_i f_j \exp\, 2\pi i(hx_j + ky_j + lz_j)\,, \qquad (1)$$

where f_j is the atomic scattering factors, h, k and l are Miller indices and x_j, y_j and z_j are the atomic partial coordinates in a unit cell.

$$\text{Zn}\,;\quad 0\,0\,0\,,\quad \frac{1}{2}\,\frac{1}{2}\,0\,,\quad \frac{1}{2}\,0\,\frac{1}{2}\,,\quad 0\,\frac{1}{2}\,\frac{1}{2}$$

$$\text{Se}\,;\quad \frac{1}{4}\,\frac{1}{4}\,\frac{1}{4}\,,\quad \frac{4}{1}\,\frac{3}{4}\,\frac{3}{4}\,,\quad \frac{3}{4}\,\frac{1}{4}\,\frac{3}{4}\,,\quad \frac{3}{4}\,\frac{3}{4}\,\frac{1}{4}\,.$$

Substituting these coordinates into eq. (1), the structure factor is obtained in the following equation.

$$F(hkl) = 4\,f_{Zn} + 4\,f_{Se} \exp\,(-in\pi/2)\,. \qquad (2)$$

The atomic scattering factors for Zn and Se layers considering the phase difference are given by

$$f_{Zn} = |\,f_{Zn}\,|\exp i\alpha_{Zn}\,,\quad f_{Se} = |\,f_{Se}\,|\exp i\alpha_{Se} \qquad (3)$$

respectively. From eqs. (2) and (3) the following formula is obtained.

$$F(hkl) = 4\,\{|\,f_{Zn}\,|\exp i\alpha_{Zn} + |\,f_{Se}\,|\exp i(\alpha_{Se} - n\pi/2)\} \qquad (4)$$

Therefore the structure factor is described as follows

$$FF^*(hkl) = 16\{|f_{Zn}|^2 + |f_{Se}|^2 + 2|f_{Zn}||f_{Se}|\cos(\alpha_{Zn} - \alpha_{Se} + n\pi/2)\} \quad (5)$$

The scattering factor corrected with dispersion by the K-electron is given by

$$f = f_0 + \Delta f'_K + i\Delta f''_K \quad (6)$$

so that

$$|f| = \sqrt{(f_0 + \Delta f'_K)^2 + (\Delta f''_K)^2} \quad (7)$$

This equation can be written quite nearly enough

$$|f| = f_0 + \Delta f'_K + \frac{1}{2}\frac{(\Delta f''_K)^2}{f_0 + \Delta f'_K} \quad (8)$$

The phase difference between the incident and the scattered radiation are derivated from eq. (6)as follows:

$$\tan\alpha_K = \frac{\Delta f''_K}{f_0 + \Delta f'_K} \quad (9)$$

where f_0 is the scattering factor for shorter waves than the wavelength of the absorption edge of the scattering element, that is, the scattering factor as usually tabulated. The values of $\Delta f'_K$ and $\Delta f''_K$, the real and imaginary parts of the correction to be applied the scattering factors on account of dispersion by K-electron, are calculated by means of Hönl's formulae.[16]

$$\Delta f'_K = \frac{2^7 e^{-4}}{9}\left\{\frac{4}{x^2(1-\delta_K)^2}\cdot \log_e|x^2-1| - \frac{1}{(1-\delta_K)^3}\left(\frac{2}{x^2} + \frac{1}{x^3}\log_e\left|\frac{x-1}{x+1}\right|\right)\right\},$$

$$\Delta f''_K = \frac{2^7 e^{-4}}{9}\pi\left\{\frac{4}{x^2(1-\delta_K)^2} - \frac{1}{x^3(1-\delta_K)^3}\right\} \quad \text{if } x > 1,$$

$$= 0 \quad \text{if } x < 1. \quad (10)$$

where x is λ_{Kabs}/λ and λ being the wavelength of the radiation scattered, λ_{Kabs} the wavelength of the K absorption edge of the scattering element, and δ_K a parameter characteristic of the scattering element.

The values of δ_K are calculated for an element of atomic number Z from the formula

$$\delta_K = (A - 911/\lambda_{Kabs})/A, \quad (11)$$

where

$$A = (Z-0.3)^2 + 1.33\times10^{-5}(Z-0.3)^4 + 3.55\times10^{-10}(Z-0.3)^6 + 11.7\times10^{-15}(Z-0.3)^8 + \cdots\cdots \quad (12)$$

The values of $\Delta f'_K$ and $\Delta f''_K$ are tabulated by W. James[16], however, the authors calculated them directly from Hönl's formulae. The necessary parameters for the present calculation of

eqs. (8) and (9) are summarized in Table I.

Table. I. Basic parameters for the calculation of diffracted intensities.

Parameters / {hkl}	$\frac{\sin\theta}{\lambda}$	f_O		A		δ_K	
		Zn	Se	Zn	Se	Zn	Se
(111) ($\bar{1}\bar{1}\bar{1}$)	0.153	25.56	28.67	892.4	1152.8	0.204	0.193
(333) ($\bar{3}\bar{3}\bar{3}$)	0.458	15.47	17.80				

Parameters / Elements	$\lambda_{K\alpha}$ (Å)	λ/λ_{Kabs}		$\triangle f_k'$		$\triangle f_k''$	
		Zn	Se	Zn	Se	Zn	Se
Rb	0.925	0.721	0.944	−0.252	−2.407	2.078	3.167
Br	1.041	0.811	1.063	−0.765	−2.962	2.536	0
Ge	1.255	0.978	1.281	−3.695	−1.912	3.428	0

From eq. (5), the diffracted intensities for the polar plane are given by

$$\begin{aligned}
FF^*(111) &= 16\{|f_{Zn}|^2+|f_{Se}|^2-2|f_{Zn}|\cdot|f_{Se}|\sin(\alpha_{Zn}-\alpha_{Se})\},\\
FF^*(\bar{1}\bar{1}\bar{1}) &= 16\{|f_{Zn}|^2+|f_{Se}|^2+2|f_{Zn}|\cdot|f_{Se}|\sin(\alpha_{Zn}-\alpha_{Se})\},\\
FF^*(333) &= 16\{|f_{Zn}|^2+|f_{Se}|^2+2|f_{Zn}|\cdot|f_{Se}|\sin(\alpha_{Zn}-\alpha_{Se})\},\\
FF^*(\bar{3}\bar{3}\bar{3}) &= 16\{|f_{Zn}|^2+|f_{Se}|^2-2|f_{Zn}|\cdot|f_{Se}|\sin(\alpha_{Zn}-\alpha_{Se})\}.
\end{aligned} \tag{13}$$

These factors can be calculated using the parameters listed in Table I. The results are shown in Table II.

Table. II. Calculated geometric scattering factors for ZnSe.

	$FF^*(111)$	$FF^*(\bar{1}\bar{1}\bar{1})$	$\frac{FF^*(111)}{FF^*(\bar{1}\bar{1}\bar{1})}$	$FF^*(333)$	$FF^*(\bar{3}\bar{3}\bar{3})$	$\frac{FF^*(333)}{FF^*(\bar{3}\bar{3}\bar{3})}$
Rb	1396	1293	1.079	441.2	504.6	0.874
Br	1151	1412	0.815	518.1	367.6	1.409
Ge	—	—	—	505.9	303.5	1.672

Actually, the values of $FF^*(hhh)/FF^*(\bar{h}\bar{h}\bar{h})$ are compared with the calculated ones. CuK_α is used to correct the setting error of the crystal and to calibrate the surface condition of the both sides of the crystal, since anomalous dispersion does not appear. The typical patterns obtained from experiment are shown in Fig. 18.

The experimental results are summarized in Table III with the calculated values. Good agreement between observed and calculated values was obtained. If the surface aspect of the both sides of the crystal were equal, and a large effective area (it was $6\times10\,mm^2$ in

this experiment) were used, the more desirable results would be expected. Comparing the results in Table IV with etching patterns, it is decided that the plane with flat bottomed pits (Fig. 13 (a), Fig. 15 (a)) corespond to $(111)_{Zn}$ or the A surfaces and small rounded pits (Fig. 13 (b), Fig. 15(b)) to $(\bar{1}\bar{1}\bar{1})_{Se}$ or the B surfaces. This conclusion is consistent with the results obtained by K. F. Burr and J. Woods about the ZnSe crystal from the vapour phase. [17]

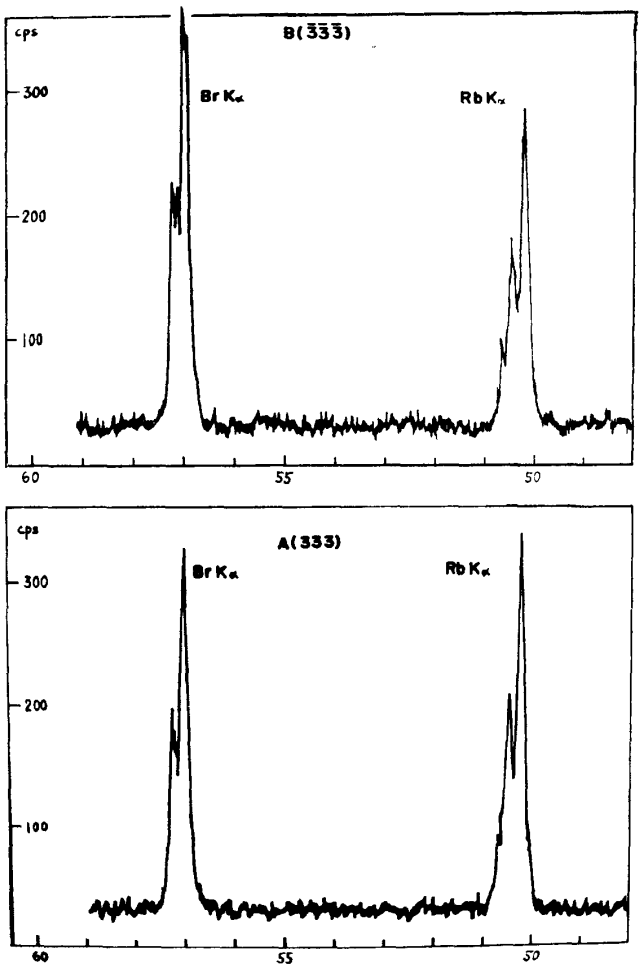

Fig. 18. X-ray {111} reflection of ZnSe with fluorescence techniques.

Table. III. Geometric scattering factors (experimental).

{hkl}	Experimental			Calc.	*Radiation*
	$FF^*(hkl)$	$FF^*(\bar{h}\bar{k}\bar{l})$	$\frac{FF^*(hkl)}{FF^*(\bar{h}\bar{k}\bar{l})}$	$\frac{FF^*(hkl)}{FF^*(\bar{h}\bar{k}\bar{l})}$	
	cps	*cps*			
(333)	218	257	0.848	0.874	Rb-K_α
(333)	282	242	1.165	1.409	Br-K_α
(333)	740	470	1.574	1.672	Ge-K_α
(333)	1960	2180	0.900	1.000	Cu-K_α
(111)	950	620	1.532	1.079	Rb-K_α
(111)	890	860	1.035	0.815	Br-K_α

§. 9. SUMMARY

The single crystals of ZnSe were grown by Bridgeman method from the melt under high inert gas pressure. The grown crystals contain many twin and twinlamellae. The width in the adjacent lamellae could be estimated from the twin boundaries on the {110} surfaces.

The evaluated width is about 30 microns along the $\langle 111 \rangle$ directions.

The etch patterns of the {110} surfaces etched slightly show the small isosceles triangular pits clearly. When the surfaces are heavily etched, the equilateral triangular pits are developed clearly. The light figure of the {110} surfaces is only observed from this heavily etched surfaces. The etch patterns of the {111} surfaces are composed of the two kinds of eqilateral triangles. The difference of these patterns can be explained by the chemical activity of the (111) and $(\bar{1}\bar{1}\bar{1})$ surfaces, *i, e.*, zinc and selenium layers. From the measurement of the ratio of diffracted intensities of X-rays $FF^*(hhh)/FF^*(\bar{h}\bar{h}\bar{h})$, the surfaces made of flat bottomed triangular pits is corespond to $\{111\}_{Zn}$ or the A surfaces and small rounded triangular pits to $\{111\}_{Se}$ or the B surfaces. This explains the process from the isoseles to equilateral triangular pits on the {110} surfaces.

Acknowledgement

The authors are deeply indebted to Dr. H. Komiya and H. Kimura of Central Research Laboratory, Mitsubishi Electric Co. for their advices on our growing the single crystal of ZnSe. We also wish to thank T. Udaka and K. Toda of Rigaku Denki Co., Ltd. for their help to our assignment of the polarity by X-rays.

References

1) A. G. Fisher: J. Electrochem. Soc. Review and News, 117 (1970) 41C.
2) S. Shionoya: Buturi 19 (1964) 612 (*in Japanese*)
3) T. Nakayama and H. Teranishi: Oyo-Buturi 39 (1970) 492. (*in Japanese*)
4) H. Kimura, H. Komiya and S. Ibuki: Mitsubishi Tech. Rept. 41 (1967) 1461 (*in Japanese*)
5) O. Eguchi and M. Fukai: National Tech. Rept. 14 (1968) 71. (*in Japanese*)
6) T. Ogawa: Buturi 17 (1962) 735. (*in Japanese*)
7) J. G. White and W. C. Roth: J. Appl. Phys. 30 (1959) 946
8) E. P. Warekois, M. C. Lavine, A. N. Mariano and H. C. Gatos: J. Appl. Phys. 33 (1962) 690.
9) J. Carides and A. G. Fisher: Solid State Comm. 2 (1964) 217.
10) M. Aven and J. S. Prener: *Physics and chemistry of II-VI compounds.* (1967), North-Holland Pub. Co.,
11) N. A. Goryunova and N. N. Fedorova: Soviet Physi Solid State 1 (1959) 307.
12) I. D. Chistyakov and E. Krucheanu: Studii Cercetari Met. 5 (1950) 517.
13) A. G. Fisher and R. J. Paff: J. Phys. Chem. Solids 23 (1962) 1479.
14) M. Yamamoto and J. Watanabe: Metal Physics 5 (1959)196. (*in Japanese*)
15) J. Hornstra: J. Phys. Chem. Solids, 5 (1958) 129.
16) W. James: *Optical principles of the diffraction of X-rays* (G. Bell and Sons, Ltd., London, 1958) Chap. IV and Appendix.
17) K. F. Burr and J. Woods: J. Cryst. Growth 9 (1971) 183.